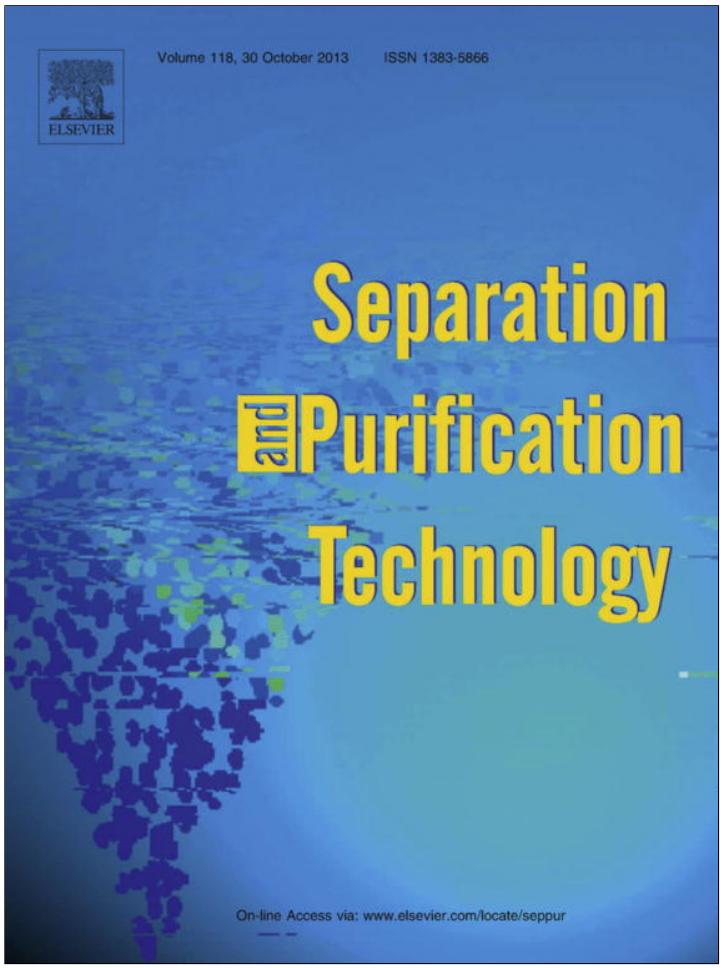
Provided for non-commercial research and education use.
Not for reproduction, distribution or commercial use.




This article appeared in a journal published by Elsevier. The attached copy is furnished to the author for internal non-commercial research and education use, including for instruction at the authors institution and sharing with colleagues.

Other uses, including reproduction and distribution, or selling or licensing copies, or posting to personal, institutional or third party websites are prohibited.

In most cases authors are permitted to post their version of the article (e.g. in Word or Tex form) to their personal website or institutional repository. Authors requiring further information regarding Elsevier's archiving and manuscript policies are encouraged to visit:

http://www.elsevier.com/authorsrights

Author's personal copy

Separation and Purification Technology 118 (2013) 762–775

Contents lists available at ScienceDirect

Separation and Purification Technology

journal homepage: www.elsevier.com/locate/seppur

# Ceramic membrane filtration of organic compounds: Effect of concentration, pH, and mixtures interactions on fouling

Laura De Angelis [a], María Marta Fidalgo de Cortalezzi [a,b,*]

[a] Departamento de Ingeniería Química, InstitutoTecnológico de Buenos Aires, Av. Eduardo Madero 399, C1106 Buenos Aires, Argentina
[b] Consejo Nacional de Investigaciones Científicas y Técnicas (CONICET), Argentina

ARTICLE INFO

*Article history:*
Received 3 April 2013
Received in revised form 8 July 2013
Accepted 13 August 2013
Available online 23 August 2013

*Keywords:*
Fouling
Ceramic membranes
Organic matter
Ultrafiltration

ABSTRACT

A comparative assessment of iron oxide ceramic ultrafiltration membranes fouling by model organic compounds was performed. To characterize this fouling phenomenon, humic acid (HA), bovine serum albumin (BSA) and sodium alginate (SA) were used as models of humic substances, proteins and polysaccharides respectively. Clean and fouled iron oxide membranes surfaces were characterized by scanning electron microscopy (SEM) and atomic force microscopy (AFM). The influence of concentration, foulant mixtures and pH on the fouling mechanism was investigated. Fouling was observed to depend first on foulant–membrane interactions, followed by a second step where membrane material plays a less important role. Membrane surface chemistry and solution pH were significant factors affecting irreversibility of the fouling layer. A strong dependence was observed in foulant concentration and solution pH. Foulant mixtures showed synergetic results, determined by foulant–foulant interactions.

© 2013 Elsevier B.V. All rights reserved.

## 1. Introduction

Membranes have been increasingly applied in the last decades in water treatment, driven mainly by new materials and improved processes. More recently, membranes have entered the waste water sector as the main component in membrane bioreactors (MBRs) [1–3]. Advantages include a smaller footprint and improved separation of microorganisms, but strong chlorine resistant membranes are required a condition many of today commercial membrane materials cannot withstand.

Ultrafiltration has proven to be an effective process from the removal of natural organic matter and more generally of organic macromolecules, such as proteins, sugars and humic substances. One of the limitations of membrane processes is the fouling that the membrane surfaces suffer during operation [4,5]. As contaminants are removed from water, they stay near or at the surface of the membrane, eventually resulting in cake formation and pore blocking. Consequences of this fouling are an increase in the pressure required for flow, more frequent chemical cleaning, and an overall deterioration of the membrane material.

There exist numerous studies in the literature that investigated the fouling of polymeric membranes by organic compounds, mainly because polymer is the material of choice for almost all current commercially available membranes for water treatment applications [6,7,5]. Developments in new materials have shifted the attention to ceramics, motivated by nanotechnology innovations and the search for catalytic surfaces. Although ceramic materials have been introduced in the water treatment industry [8–10], very little is known about the fouling characteristics of these membranes by organic macromolecules. Therefore in order to advance the use of ceramics membranes, it is necessary to understand the chemical and physical phenomena involved. Commercially available ceramic membrane materials include alumina, titania, zirconia, and silicon carbide. They are composed of an extruded support material (alumina in most cases) onto which a thinner layer (effective separation layer) of a second material has been deposited generally by dip-coating or spin coating particles. Key issues in achieving a good asymmetric ceramic membrane are precursor particle size distribution, as it is directly related to the final membrane pore size, and support-skin material compatibility, as it is required to ensure adherence of the two layers.

Previous attempts to incorporate iron oxide on membranes, both ceramic and polymeric, include coating of microfiltration membranes with ferrihydrate nanoparticles [11], layer by layer deposition [12,13] or filtering [14] of alpha-$Fe_2O_3$ nanoparticles, and sol–gel techniques [15], and may include a final sintering step if the support material withstands high temperatures. Improvement in natural organic matter (NOM) removal by iron oxide coated membranes was detected for the adsorbing fractions, although long term fouling may be a problem if an appropriate cleaning strategy is not implemented [13].

* Corresponding author at: Departamento de Ingeniería Química, InstitutoTecnológico de Buenos Aires, Av. Eduardo Madero 399, C1106 Buenos Aires, Argentina. Tel.: +54 11 6393 4862; fax: +54 11 6393 4860.
*E-mail addresses:* ldeangel@itba.edu.ar, mfidalgo@itba.edu.ar (M.M.F. de Cortalezzi).

1383-5866/$ - see front matter © 2013 Elsevier B.V. All rights reserved.
http://dx.doi.org/10.1016/j.seppur.2013.08.016

Author's personal copy



Researchers [16–18] have made a distinction between foulant–foulant and foulant–membrane surface interactions as regard to their net effect on the overall fouling process during operation. Therefore, it is expected that ceramic membranes should suffer an initial and distinctive fouling phase where specific foulant–membrane material interactions dominate, followed by a second phase with behaviour similar to that reported in the literature for polymeric membranes [19]. Inherent characteristics of the feed solution, such as concentration, pH and concomitant effects also appear to play a significant role in the process.

We have previously reported on a novel fabrication process for iron-oxide ceramic membranes [20], derived from an organic acid stabilized nanoparticles (ferroxanes) with rejection capabilities in the ultrafiltration range. The ferroxane nanoparticles were successfully cast onto alumina supports fabricated in different geometries (tubular, disc, etc.) as required for specific uses. The introduction of a new, chemically active material for ceramic membranes opens a broad range of application possibilities, such as adsorbents [21], disinfectants [22], or catalysts [23]. Additionally, the precursor particles are synthesized in aqueous media and low to moderate temperatures are required throughout membrane fabrication. This results in significant improvements over other preparation methods reported with respect to environmental and economic aspects, one of the main drawbacks of ceramic membranes today compared with their polymeric counterparts. In spite of their promising outlooks, the fouling characteristics of iron oxide ceramics membranes have not yet been investigated.

The purpose of the present study is to examine the complex phenomena of iron ceramic membrane fouling by organic compounds. The fouling potential of NOM, proteins, and polysaccharides was investigated by three model organic compounds: humic acid, bovine serum albumin, and alginic acid respectively. These substances adequately represent chemical compounds commonly encountered in surface waters and/or mixed liqueur biological reactors, where ceramic membranes may be used for drinking water treatment or wastewater MBR's.

Membrane permeability was analyzed for various foulant concentrations and feed solution pHs. Different pH values were investigated above and below membrane point of zero charge to assess electrostatic membrane–foulant interactions. In addition, as natural waters are a complex mixture of substances, combined fouling was studied and compared to single foulant behaviour.

## 2. Theory

Theoretical models of membrane fouling recognize four mechanisms: complete blocking, standard blocking, intermediate blocking, and cake formation.

Complete blocking occurs when particles arriving at the membrane surface result in blocking of one or more pores with no superposition of the particles. The flow as a function of filtration time can be represented by:

$$J = J_0 e^{-At} \tag{1}$$

where $A$ is

$$A = K_A u_0 \tag{2}$$

and $K_A$ is the membrane surface blocked per unit of total volume permeated through the membrane, and $u_0$ is the mean initial velocity of the filtrate.

If the particles arriving at the surface deposit onto the internal walls, causing a decrease in the pore volume of the membrane, the standard blocking phenomenon is present. In this case, the evolution of flow with time is given by

$$J = \frac{J_0}{(1 + Bt)^2} \tag{3}$$

where $B$ is

$$B = K_B u_0 \tag{4}$$

and $K_B$ is the decrease in cross section area of the pores due to the particles deposited on the walls per unit of total permeate volume.

The intermediate blocking phenomenon refers to the situation where each particle can either settle on other particle already deposited or block directly some membrane area. The corresponding volume versus time functional dependence is

$$J = \frac{J_0}{(1 + At)} \tag{5}$$

Lastly, the fouling process evolves into a situation where there is no room to directly obstruct the membrane and all new particles arriving deposit onto already settled particles. This mechanisms is called cake filtration, and the flow-time relationship is given by

$$J = \frac{J_0}{\sqrt{1 + Ct}} \tag{6}$$

where $C$ is

$$C = (2R_r)K_C u_0 \tag{7}$$

and $K_C^{-1}$ is the total permeate volume per unit of membrane area and $R_r$ is the ratio of the resistance of the cake to the clean membrane resistance.

During the course of a filtration experiment, the complex process of flux decline is expected to be modelled not by a single mechanism, but rather by some or all of these processes that act sequentially. When the size of the solute is greater than the mean pore size of the membranes, total rejection would lead to complete blocking rapidly evolving into cake formation once a layer of foulant has been deposited onto the surface.

On the other hand, if solute size is much smaller that mean pore size, a standard blocking mechanism is expected, followed probably by intermediate blocking before shifting to cake formation. The intermediate situation arises when the sizes of pores and solute are comparable; in this case, a combination of complete, standard, and intermediate blocking should appear, and the relative influence of each one will depend on the pore size distribution of the membrane.

## 3. Materials and methods

### 3.1. Chemicals

Iron oxide nanoparticles were synthesized in the laboratory from industrial grade $FeCl_2$ (28–32% w/w) obtained from PPE Argentina S.A. and anhydrous acetic acid (Anedra, Argentina).

Molecular weight cut off (MWCO) test solutions were prepared with the following concentrations of dextran fractions (Sigma Chemical Co.): 0.25 wt% T-10 (average molecular weight 11,600), 0.10 wt% T-50 (avg. MW 48,600), 0.10 wt% T-150 (average MW 148,000), 0.20 wt% T-400 (average MW 410,000) and 0.20 wt% T-700 (average MW 668,000). Sodium Azide (99%, Aldrich) was added at a concentration of 0.05 wt% to prevent bacterial growth and sodium chloride (NaCl) 0.05 M to inhibit interaction between molecules and surfaces. Ultrapure water was used in all the experiments (18 MΩ quality).

Reagents used in fouling and cleaning processes were of analytical grade, with the exception of the Humic Acid sodium salt (HA) (Sigma–Aldrich, technical grade). Bovine Serum Albumin (BSA) (98%) and Sodium Alginate (SA) were obtained from Sigma–Aldrich Company; NaOH and HCl (Anedra, Argentina) were used for pH adjustment.

Author's personal copy



### 3.2. Fabrication of ferroxane derived membranes

Ferroxane nanoparticles were obtained by lepidocrocite (γ-FeOOH) reaction with acetic acid, deposited onto alumina supports, and then fired to attain a porous layer [20]. Briefly, γ-FeOOH (lepidocrocite) was synthesized from the oxidation of $FeCl_2$ under controlled pH conditions [24]. Secondly, lepidocrocite was reacted with acetic acid at room temperature to obtain the organically-coated ferroxane particles, and a significant decrease in size was achieved.

Alumina supports were fabricated in the laboratory by pressing of powdered alumina in a custom made stainless steel mold and sintering at 1100 °C.

Following purification and drying of the ferroxane particles, the composite membranes were fabricated by dip-coating of flat porous alumina supports with a concentrated suspension of the iron oxide precursor.

The coated supports were dried and sintered at a maximum temperature of 350 °C for at least 4 h, to produce full conversion of the ferroxane particles to hematite. The fabrication method selected was devised to obtain high reproducibility of membrane uniformity, thickness and permeability.

### 3.3. Filtration experiments

The filtration experiments were performed in dead-end mode, in a custom made cell under constant pressure conditions, supplied by compressed air.

Permeate flux of both as-prepared and fouled membranes were determined by clean water filtration experiments. Permeate volume was recorded over time and flux determined as the slope of the linear fit of the experimental data from Darcy's following equation:

$$J = \frac{dV}{dt \cdot A} = \frac{\Delta P}{\mu \cdot R_T} = \frac{\Delta P}{\mu \cdot (R_m + R_f)} \tag{8}$$

where $J$ is the permeate flux, $A$ is the effective filtration area, $\Delta P$ is the transmembrane filtration pressure, $\mu$ the solution viscosity and $R_T$ is the total membrane hydraulic resistance.

The net hydraulic resistance due to fouling ($R_f$) was defined as the difference between the total hydraulic resistance ($R_T$) and the clean membrane resistance ($R_m$)

$$R_f = \left(\frac{\Delta P}{\mu \cdot J}\right) - R_m \tag{9}$$

where

$$R_m = \frac{\Delta P}{\mu J_0} \tag{10}$$

$R_m$ can be obtained by filtering water through a clean membrane, when $R_f$ is zero.

MWCO experiments were performed following a protocol based on the American Society for Testing and Materials (ASTM) publication E 1343-90 (97). Briefly, solutions of dextran molecules with molecular weights ranging from 10,000 g/mol to 600,000 g/mol were filtered through the membrane. Concentrations of both feed and permeate solutions were determined by Total Organic Carbon (TOC) analysis for each dextran fraction and a rejection level was determined for each molecular weight. TOC was analyzed in a Shimadzu TOC Analyzer, TOC-VCPH, equipped with an ASI-V auto sampler (Kyoto, Japan).

### 3.4. Membrane material characterization

The specific surface area, charge, and morphology of the iron-oxide material, which comprises the upper, active layer of the membrane, were investigated. For these measurements, unsupported ceramics were fabricated, drying concentrated suspensions of ferroxane particles to obtain a homogeneous green body, and then following the same protocol as used for the supported membranes.

The specific surface area was measured by Brunauer–Emmet–Teller (BET) $N_2$ adsorption method and the pore size was calculated by the Barret, Joyner and Halenda (BJH) $N_2$ adsorption/desorption isotherm method at 77 K using a Coulter™ SA 3100™ (Beckman Coulter, USA) analyzer.

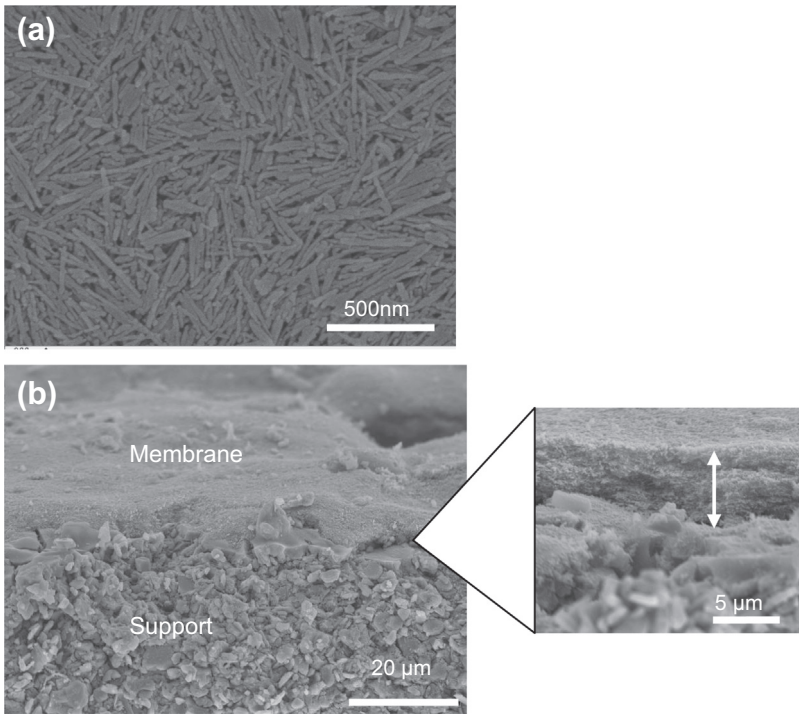



**Fig. 1.** SEM images of iron oxide ceramic membranes; (a) top view; and (b) cross sectional view.

Author's personal copy



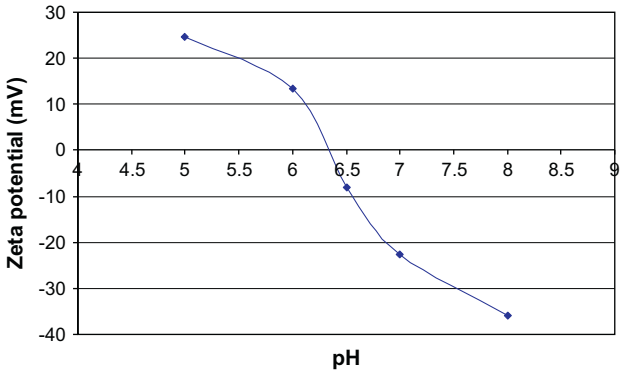



**Fig. 2.** Zeta potential vs. pH plot for iron oxide ceramic membrane.

The surface charge of the membrane was investigated through zeta potential measurements using a Malvern Nanosizer ZS (Malvern Instruments, UK).

Both clean and fouled membranes surfaces were imaged by scanning electron microscopy (SEM) (PHILIPS XL30 TMP New Look). Atomic Force microscopy (AFM) scans were obtained in a Multimode Scanning Probe Microscope Nanoscope IIIa (Digital Instrument-Veeco, Santa Barbara, CA) in tapping mode. AFM images were analyzed with WSxM 3.0 Beta 11.5 (Copyright Nanotec Electronica S.L.) AFM Software.

## 4. Results and discussion

### 4.1. Membrane characterization

Clean water flux was measured for both the membrane and support material alone. A decrease in the permeability of the asymmetric membrane was observed with respect to the support as expected, but it still retained good flux. Average measured fluxes at a transmembrane pressure of 50 kPa were $1500 \pm 70$ L/m$^2$h for the support material and $1000 \pm 40$ L/m$^2$h for the asymmetric iron oxide membrane.

SEM images of the as-prepared, "clean" membrane top surface and cross section are shown in Fig. 1a and b respectively. The elongated "needle-like" shape of the precursor ferroxane nanoparticles could still be distinguished, giving a highly rough appearance. The cross-sectional view allowed differentiating the top layer from the coarser grains of the support material. The thickness of the iron-oxide coating was approximately 5 μm. Determinations along the cross-section indicated that uniform coatings were achieved, with no significant thickness variations within the experimental error of the measuring technique.

Nitrogen adsorption isotherms of iron-oxide unsupported ceramics indicated a BET specific surface area of $41.88 + -5.42$ m$^2$/g. The average pore size was determined to be 75 nm, with a standard deviation of the pores size distribution of 10 nm. The relatively narrow pore size distribution stems from the low polydispersity of the ferroxane nanoparticles used as ceramic precursors [20].

Surface charge is expected to play a significant role in the fouling by charged molecules. Zeta potential measurements were conducted for five pH levels between 5 and 8 (Fig. 2). The ferroxane derived membrane showed a pzc of 6.3, consistent with other reported values for hematite in the literature [25]. The absolute value of the zeta potential increased rapidly as pH shifted towards higher or lower levels.

The AFM scans of the membrane surface accurately revealed the features discussed previously (Fig. 3). Surface roughness was analyzed from AFM scans, in 5 μm × 5 μm spots. The height distribution histogram from a total of 1000 data points over the 25 μm$^2$ surface showed a centered peak at 350 nm, which corresponds to the most frequent pore depth in the analyzed sample surface. Surface pore size measurements were conducted from readings of twenty cross-sectional profiles as shown in Fig. I, Supplementary information, measuring a minimum of 3–4 pore openings for each line. The average pore opening size at the surface was determined to be 150.3 nm with a standard deviation of 59.8 nm. Given the inherent limitations of AFM scans to determine surface pore sizes [26] (inability of the AFM probe to follow surfaces with abrupt height differences, and/or narrow openings) the results are in reasonable agreements with those from nitrogen adsorption isotherms. It is important to point out that both techniques will detect all porosity, regardless of actual pore connectivity through the material. In this sense, they become an upper limit for the pore volume of the membrane, as some area and pore entrances accounted for in these measurements will not effectively contribute to transport and therefore offer no true area for flow through the filter.

Dextran fraction filtration experiments yielded a MWCO between 130,000 g/mol and 180,000 g/mol, with an average value of 150,000 g/mol, corresponding to the ultrafiltration range. The complete rejection vs. molecular weight curve is depicted in Figure II in the Supplementary data. This result is in good agreement with previously reported values for this material [20].

### 4.2. Membrane fouling

Three different model organic compounds were used in fouling experiments: humic acid (natural organic matter), bovine serum albumin (protein), and sodium alginate (polysaccharide) to investigate the relative fouling capacity of each one, and their combined effects on iron-oxide ceramic membranes.

Flux decline, hydraulic cleaning, and fouling reversibility were investigated. By comparing the values measured for clean water and fouled-membrane permeability, an assessment of the fouling potential of each type of compound was obtained. In all experiments there was a rapid decline in flux, indicating the onset of fouling.

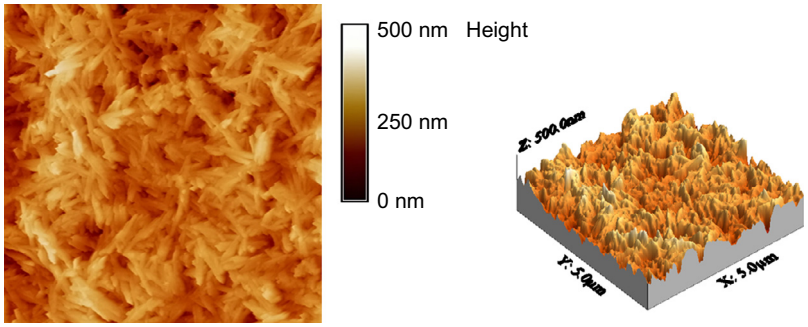



**Fig. 3.** AFM scans of ferroxane derived membrane; top view and 3-D view.

Author's personal copy



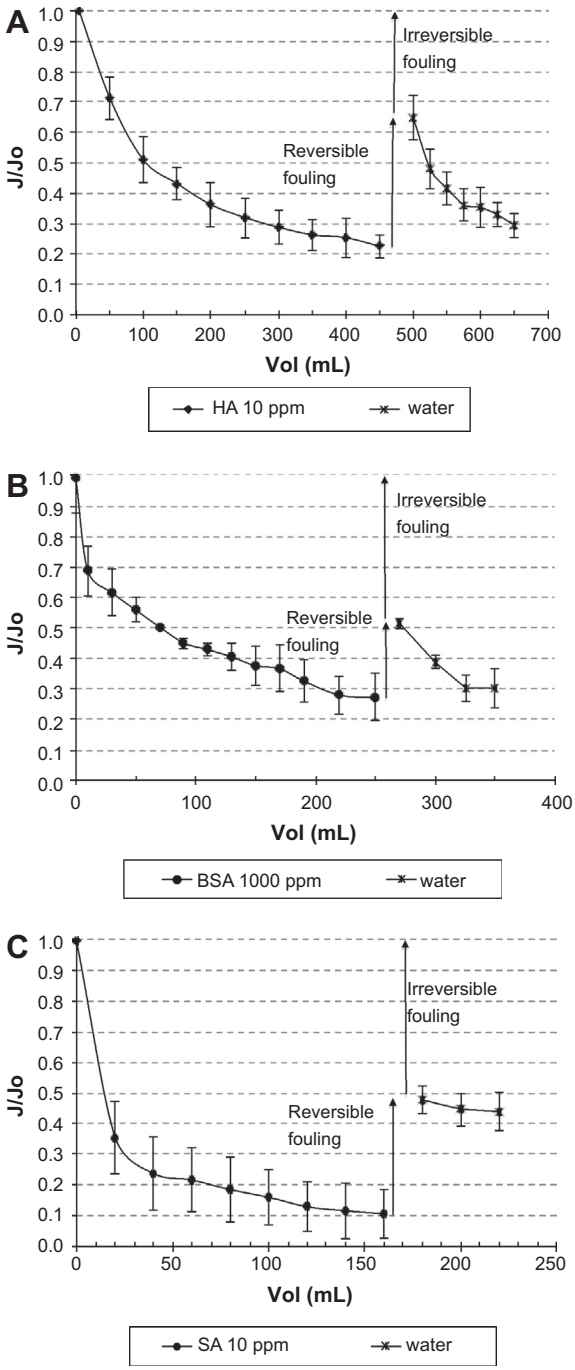



**Fig. 4.** Normalized flux decline vs. total volume filtered for each foulant and clean water flux after simulated hydraulic cleaning; (a) [HA] = 10 ppm; (b) [BSA] = 1 g/L; (c) [SA] = 10 ppm. $\Delta P$ = 0.5 bar, pH = 7. *I*: irreversible fouling. *R*: reversible fouling.

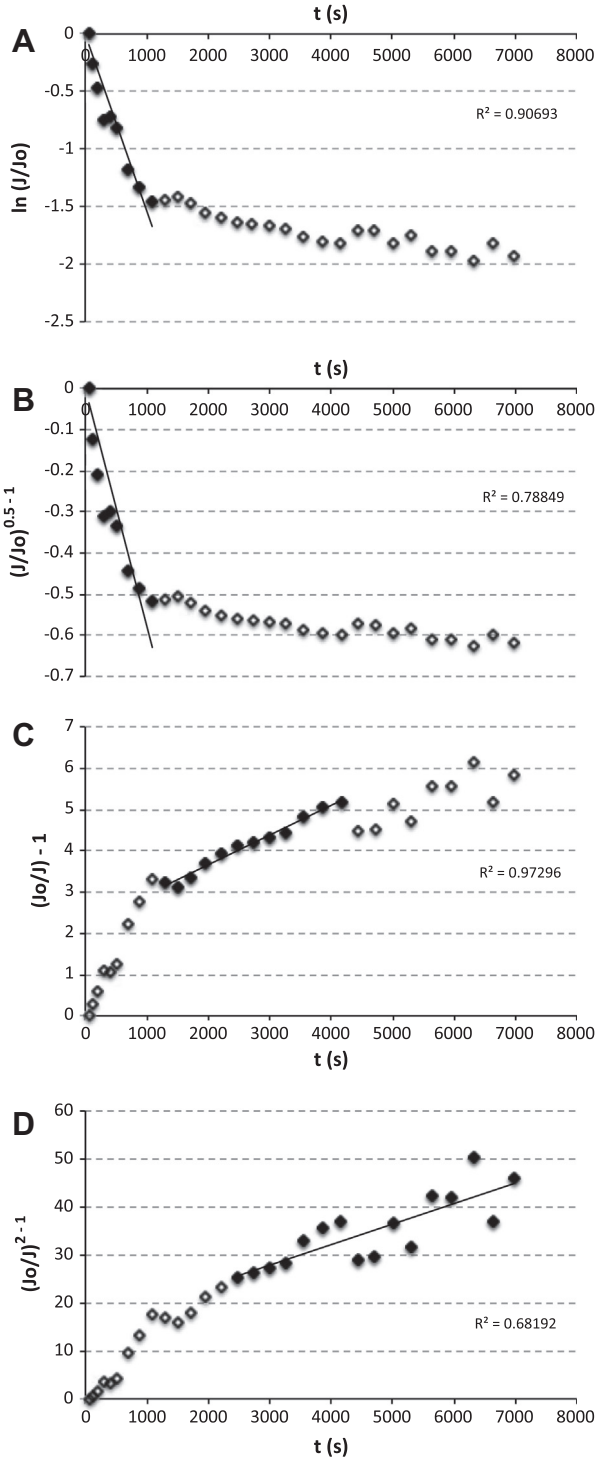



**Fig. 5.** Analysis of the HA filtration experiments from the linear expressions of the classical modelling mechanisms: (A) complete blocking; (B) standard blocking; (C) intermediate blocking; and (D) cake filtration. $R^2$ coefficients correspond to the linear regression fitting of the solid marker data points.

After the initial fouling stage, the membranes were rinsed thoroughly with ultrapure water to simulate a hydraulic cleaning followed by a second measurement of the filter permeate flux to assess the degree of irreversible fouling [27]. Solutions were filtered up to the point where the 70% reduction of initial flux was exceeded, with the exception of the SA experiment that was stopped at 150 ml due to severe fouling. Foulant concentrations used were 10 ppm for HA and SA, and 1000 ppm for BSA, based on previous reports in the literature and the fouling potential expected [4,28]. BSA filtration experiments at 10 ppm were also conducted in order to compare fouling potential at the same concentration for the three compounds. However, fouling observed in this last case was minimal, and therefore all further protein experiments were conducted at relatively higher concentrations. The compounds were dissolved in ultrapure DI water and pH adjusted to 7 by addition of NaOH. Concentrations higher than the average content of typical natural water were chosen in order to accelerate the fouling process. Feed solution volumes between 200 ml and 500 ml were filtered at each experiment, with the exception of the low concentration protein solution, when a total of 2000 ml were filtered.

Author's personal copy



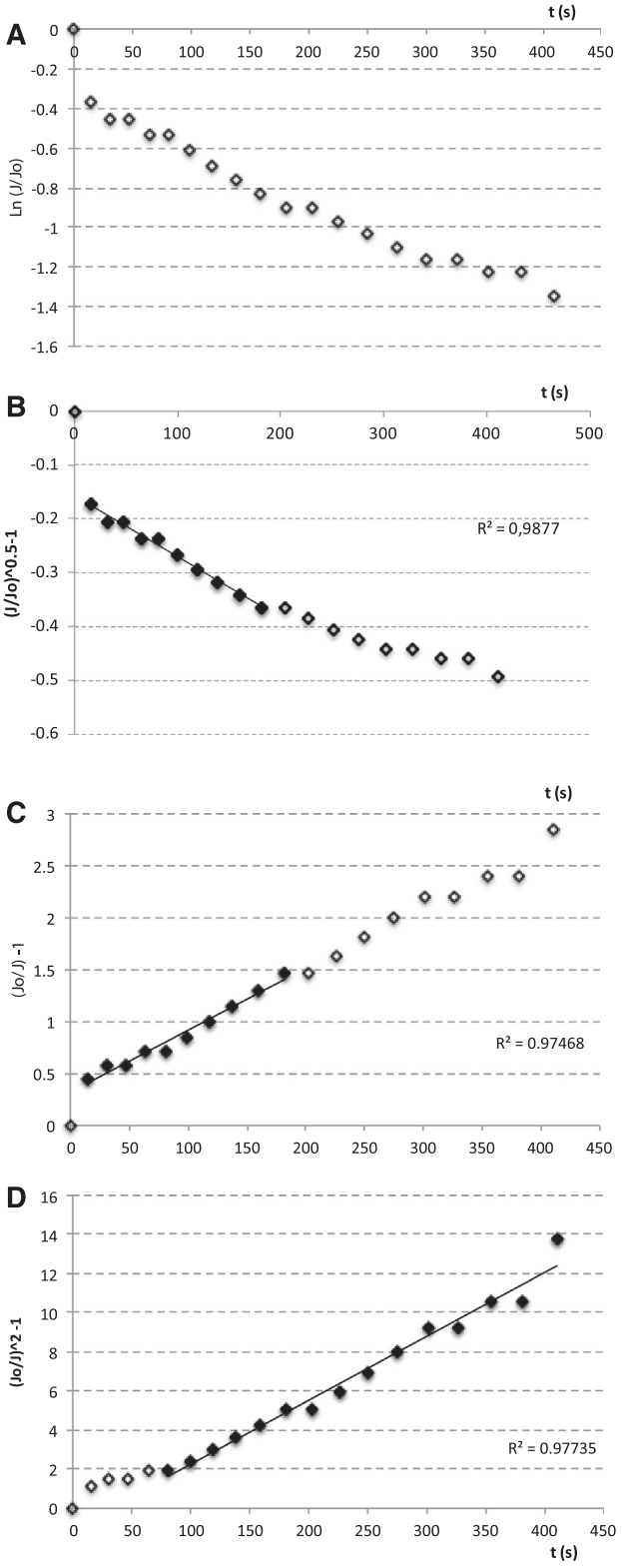



**Fig. 6.** Analysis of the BSA filtration experiments from the linear expressions of the classical modelling mechanisms: (A) complete blocking; (B) standard blocking; (C) intermediate blocking; and (D) cake filtration. $R^2$ coefficients correspond to the linear regression fitting of the solid marker data points.

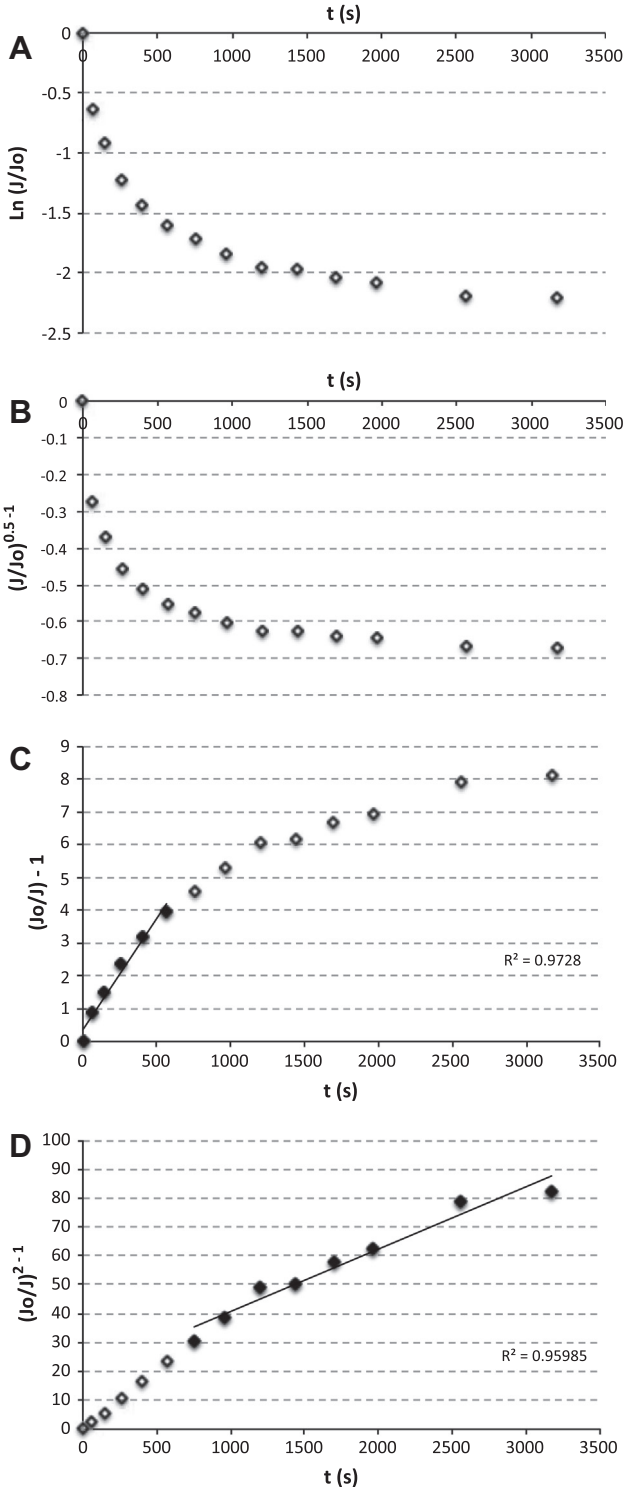



**Fig. 7.** Analysis of the SA filtration experiments from the linear expressions of the classical modelling mechanisms: (A) complete blocking; (B) standard blocking; (C) intermediate blocking; and (D) cake filtration. $R^2$ coefficients correspond to the linear regression fitting of the solid marker data points.

Several theoretical models of flow reduction based on blocking mechanisms have been proposed. These models describe four possible mechanisms: complete blocking, standard blocking, intermediate blocking and cake filtration [29,30]. Usually, individual models cannot completely explain the flux evolution over time, but rather a combination of mechanisms is present. The size of the solutes relative to the pores of the membrane will determine the extent at which each mechanism is present and its progression. For molecules smaller than the mean pore size, an initial phase dominated by standard blocking first and intermediate blocking later is expected, followed by a transition to cake filtration at a

Author's personal copy



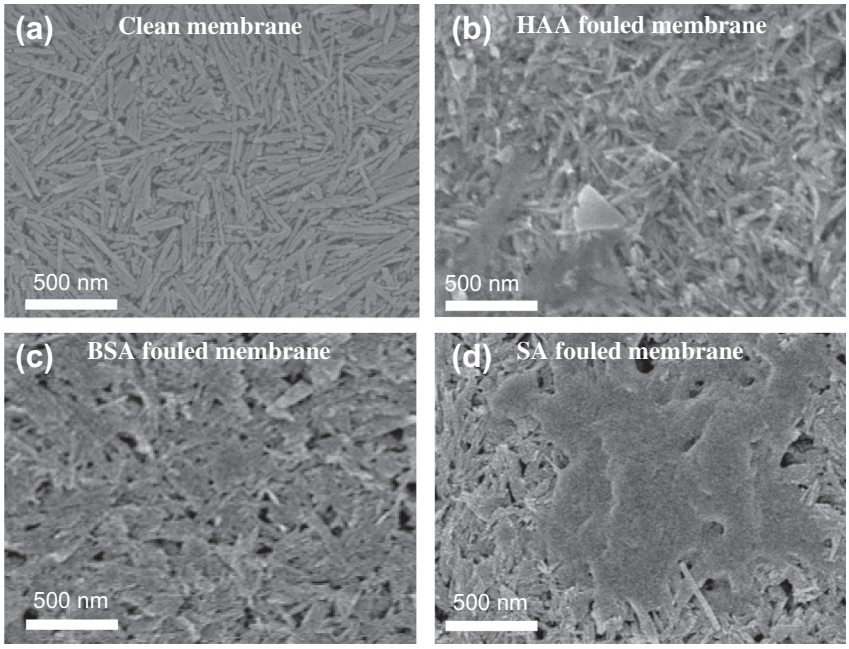



**Fig. 8.** SEM images of the top surface of a ferroxane derivate membrane: (a) clean membrane; (b) HA-fouled membrane; (c) BSA-fouled membrane; and (d) SA-fouled membrane.

subsequent stage in the process. This is the case for HA (MW 10–50 kDa as determined by SEC, and Stokes radius 3–7 nm [31] and BSA (MW 66.7 kDa reported by the manufacturer and Stokes radius 3.5 nm) [32], with a solute to pore size ratio of 0.07 and 0.09. It is important to highlight that molecular configuration and electrostatic expansion of the molecules may be affected by concentration, pH, and ionic strength values, as well as membrane surface interactions, and therefore actual results should be analysed considering the variations of these parameters. On the other hand, solutes of sizes larger than the membrane pores, like SA (120–190 kDa) are expected to follow a pattern consisting of the fast formation of a concentration polarization layer due to total retention, evolving rapidly into cake formation [28].

Linear relationships based on the acting mechanism time laws were calculated in order to analyse the applicability of each one. The data was then plotted following the four obtained relationships and linear regression equation and coefficient of determination was calculated. The methodology allowed for the identification of the main operational mechanism and its modifications, if any.

Fig. 4 presents the results for the fouling experiments. Error bars show standard deviation from at least triplicate experiments. In all cases, the dispersions of numerical results obtained were below 10%. Experimental data was fitted to the four classical mechanisms proposed for fouling, through plots of the linear form for time dependency of flow. Figs. 5–7 depict the plots of the expressions corresponding to linear relationships for the acting mechanisms, as well as the coefficient of determination $r^2$ when applicable.

At the beginning of the HA solution filtration (Fig. 4A), a sharp flux reduction was observed, attributable to pore blocking, followed by a flattening of the slope suggesting the formation of a cake. After cleaning with water, the 56% of the flux decay was recovered, but as pure water passed through the membrane again, it dropped sharply. The strong and well-documented iron oxide–HA interaction seems to be responsible for the irreversible part of the fouling; the hydraulic treatment did not effectively removed the foulant from the surface due to the affinity between the compounds, leading to a rapid blocking of the pores after filtration is resumed and pressure is re applied.

The first stage of the filtration experiment could be accurately described by the complete blocking mechanism expression (Fig. 5) up to 1000 s or 225 ml, while after this point the predominant mechanism was intermediate blocking, followed by cake filtration in the last part of the experiment due to the accumulation of solute near the surface of the membrane. The fact that complete blocking provided a better model for the experimental data than standard blocking, as expected from the molecular size and the average pore size of the membrane hints to the possibility that aggregation of the HA and hydrophobicity caused them to effectively behave as a larger molecule. At pH 7, both HA and the membrane are negatively charged, and so electrostatic repulsion will contribute to increase rejection and build up of material at the interface. Adsorption on the surface of the membrane could also explain partially this observation: the highly rough ceramic surface exposes a large area at the membrane/solution interface, and deposition of adsorbed molecules on elongated surface pore openings may lead to pore constriction on the surface and therefore increase retention.

In the BSA filtration experiments (Fig. 4B), a more accentuated effect of the initial fouling was observed than in the previous case. Iron oxide–foulant interaction appeared to be stronger than for HA; electrostatic forces were expected to favour adsorption of BSA to the membrane at pHs close to the point of zero charge, leading to a higher degree of irreversible fouling [8]. After surface rinsing with ultrapure water, the flux recovery was minimal; the same flux decrease was observed and no long-term recuperation was achieved, as a result of the strong adsorption of the protein to the iron oxide. It can be concluded that high molecular weight components like BSA with polar groups near the membrane surface cause significant flux decline within a relatively short filtration time. Experimental data adjusts well to standard and intermediate blocking mechanisms (Fig. 6) indicating adsorption onto the inner pores of the membrane. The relatively high concentration used in the experiments may be the reason for a rapid turn to intermediate blocking and cake filtration, due to the formation of a

Author's personal copy



concentration polarization layer on the surface of the membrane. The large fraction of irreversible fouling observed is also consistent with the proposed dominant mechanism of inner pore adsorption with particle superposition due to material accumulation near the surface of the membrane. In order to isolate this effect, additional filtrations were conducted at an initial concentration of BSA of 10 ppm, creating a situation equivalent to the one investigated for the other molecules (Fig. IV, Supplemental information). Interestingly, while fouling was much retarded as expected from a 100-fold decrease in feed concentration, the ratio of reversible to irreversible fouling was conserved: in both cases, 29% of the flux declined was reversible while 70% was irrecoverable by hydraulic cleaning.

The SA filtrations showed a sharp flux drop at the beginning (Fig. 4C), to almost 20% of the clean water flux after only 50 ml filtered. A similar behaviour has been reported for alginate filtration with polymeric organic membranes [33,28], associated with the rapid formation of a gel-like layer on the membrane leading to a complete blockage of the surface. After rinsing the SA fouled membrane with ultrapure water, recovery was approximately 50% of the initial flux. This is attributable mainly to the high solubility of polysaccharides in water, and the re-dissolution of the gel layer. Reversible fouling accounted for almost half (44%) of total flux reduction. However, as clean water filtration is resumed, no change in the permeability was observed with time, indicating the residual fouling layer did not suffer any loss of porosity by compaction that may result in an increased hydraulic resistance. Opposite behaviour was observed for HA and BSA, where irreversible loss of permeability was aggravated by further compression of the fouling layer during clean water filtration.

Interpretation of the experimental data with the mechanistic models are consistent with a first stage of intermediate blocking, where particles block the surface pores but also deposit onto each other, followed rapidly (570 s or 60 ml) by a well defined cake filtration mechanism (Fig. 7). This point corresponds to the end the initial large decay observed in the flux evolution with time, and the beginning of a considerably slower reduction of permeability.

Membrane–foulant interactions can be inferred from the relative importance of the irreversible part of the fouling, that accounted for approximately half of the flux reduction both for HA and SA, but escalated to 70% for BSA. It can be explained by the hydrophilic character of the iron oxide that translates in a higher affinity for the polar proteins than the hydrophobic humic substances. The observation is directly opposite to the report of fouling of hydrophobic polyethersulfone membranes by HA and alginate, where the first one caused mainly irreversible fouling and the latter a relatively reversible one [34].

The surface images by SEM showed the differences between clean membrane and organic matter-fouled membrane (Fig. 8), after the simulated hydraulic cleaning. Both the HA and BSA fouled membrane showed limited coverage of the surface, while the clean membrane morphology could still be partially seen (Fig. 8b and c). Fig. 8d showed the gel layer formed after fouling with SA, resulting in an area of complete blockage of the surface porosity.

HA fouled membranes were further characterized by AFM (Fig. III, Supplementary information). Attempts to characterize BSA and SA fouled membranes in the same fashion failed due to particles being removed from the surface of the membrane and attached to the cantilever. Image quality is heavily affected by tip contamination, and hence no reliable information could be extracted from those scans. Analysis of HA fouled membrane images revealed a reduction in the relative roughness, from a root mean square (RMS) roughness for the clean membrane of 71 nm to a fouled membrane roughness of 35 nm, along with a pore depth reduction, from 350 nm in the clean membrane to 100 nm in the fouled case, due to the deposit of HA inside the pore valleys [35], resulting in significant flattening of the topology.

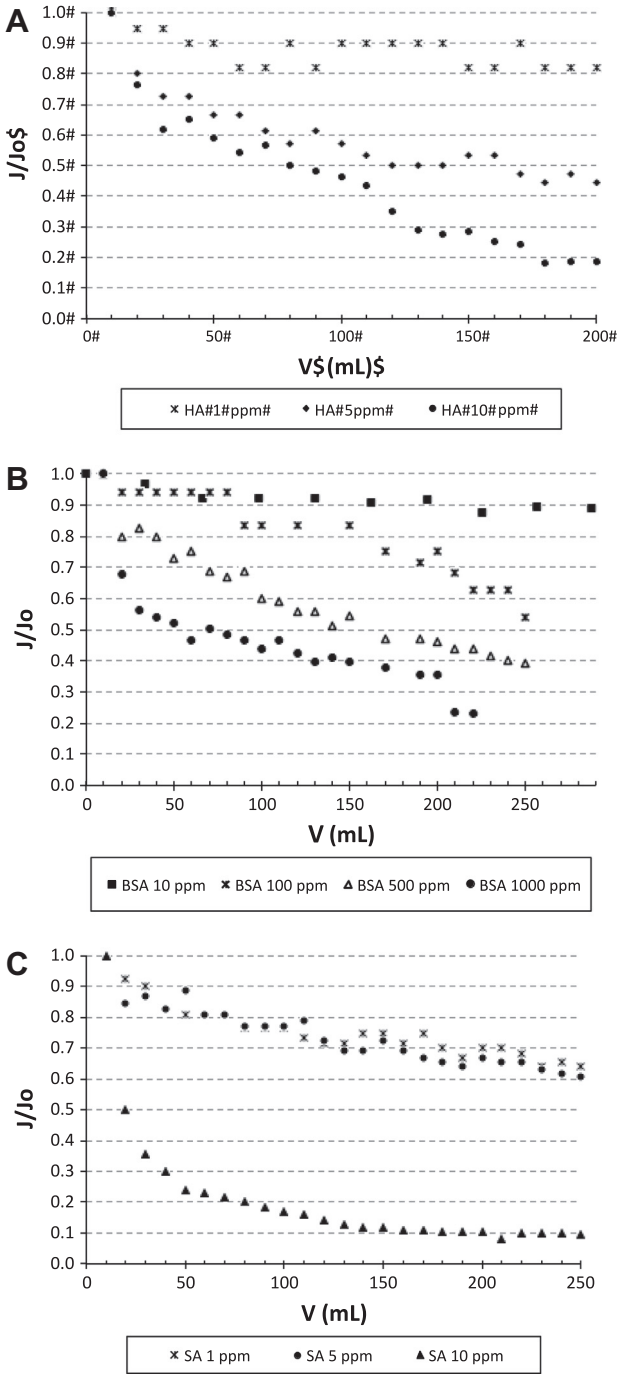



**Fig. 9.** Normalized flux decline as a function of volume filtered for different foulant concentrations; (A) [HA] = 1 ppm, 5 ppm, and 10 ppm; (B) [BSA] = 10 ppm, 100 ppm, 500 ppm, and 1000 ppm; (C) [SA] = 1 ppm, 5 ppm, and 10 ppm; $\Delta P$ = 0.5 bar, pH = 7.

### 4.2.1. Effect of foulant concentration

To investigate how the feed foulant concentration affects the membrane flux profile, filtration experiments were performed under the following conditions: 1 ppm, 5 ppm, and 10 ppm HA; 10 ppm, 100 ppm, 500 ppm, and 1000 ppm BSA; and 1 ppm, 5 ppm, and 10 ppm SA. The compounds were dissolved in ultrapure DI water and pH adjusted to 7, by addition of NaOH.

Author's personal copy



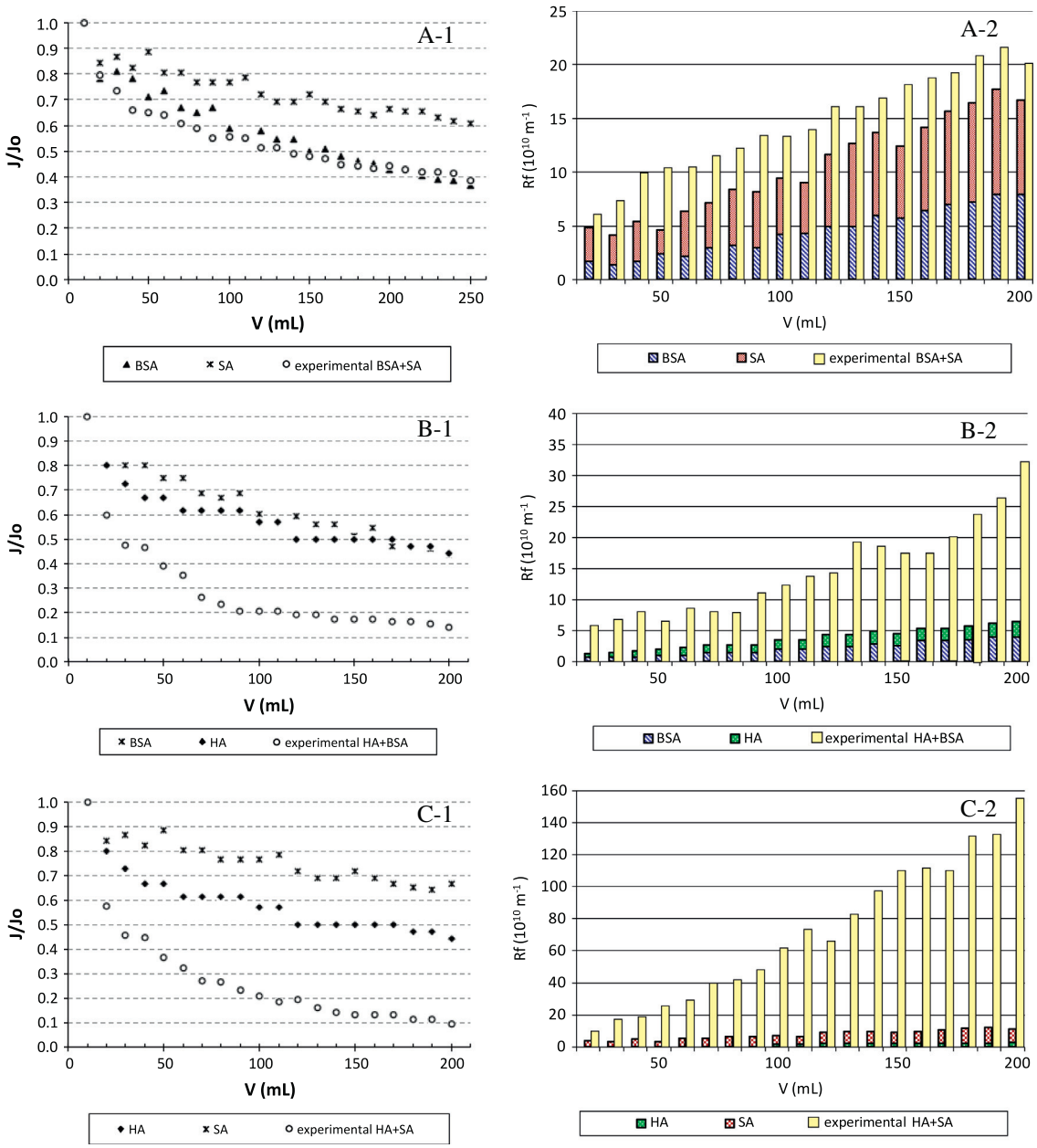



**Fig. 10.** (1) Normalized permeability and (2) calculated fouling layer hydraulic resistance from single compounds and mixtures for the filtration experiments of single compounds BSA (500 ppm), HA (5 ppm), and SA (5 ppm) and mixtures filtration of same concentrations; $\Delta P = 0.5$ bar; pH 7.

Fig. 9 shows measured membrane flux as a function of organic foulant concentration. In general, a positive correlation was observed between fouling and concentration increase in the feed.

During filtration of 1 ppm HA (Fig. 9A), minimum fouling was found, only 20% flux reduction after 200 ml filtration. For 5 ppm and 10 ppm concentrations, the same filtrated volume produced a flux reduction of 60% and 80%, respectively. This can be attributed to pore obstruction due to the interaction between humic acid and iron oxides, since HA is known to adsorb onto iron oxides surfaces through its polar functional groups (carboxyl and hydroxyl groups) [25].

This behaviour could be found also in the BSA case for all concentrations, with a steepest descent at the initial stages of the filtration, when fouling was dominated by protein–iron oxide interactions. BSA exhibits high affinity for the membrane surface, mainly due to the presence of amino-acid groups. After this initial stage, fouling continued through protein–protein interactions, giving a steady decrease of the normalized flux. Foulant deposition rate can be related to flux decline rate, which in turned is governed by membrane–foulant interactions and after the formation of a monolayer on the filter surface, foulant–foulant interactions [27]. The results hint to a strong iron oxide–BSA interaction, comparable to BSA–BSA interaction forces, underlining the observation of fouling irreversibility discussed in the previous section.

For SA concentrations under 10 ppm, no significant concentration effects were observed. For higher concentrations, the fouling rate increased drastically. Modelling of the SA filtration data (Fig. V, Supplementary information) showed a distinct curve shape for the 10 ppm situation with respect to the other two solutions. The non-linearity of the plotted data for complete and standard blocking mechanism in Fig. V A and B, clearly points to the intermediate blocking followed by cake filtration. However, the first

Author's personal copy



two mechanisms cannot be ruled out as contributors to fouling for the lower concentration experiments. This can be explained by the accumulation of SA at or near the surface of the membrane, that rapidly reached the level at which a gel like structure is formed [33], causing the complete blocking of the pores on the membrane.

*4.2.2. Effect of foulant mixtures*

The concomitant effect of humic acids, serum albumin and sodium alginate was investigated. Mixture effects are of great interest for analysis, since in actual water systems, contaminants are found in complex mixtures, rather than individually. The combined

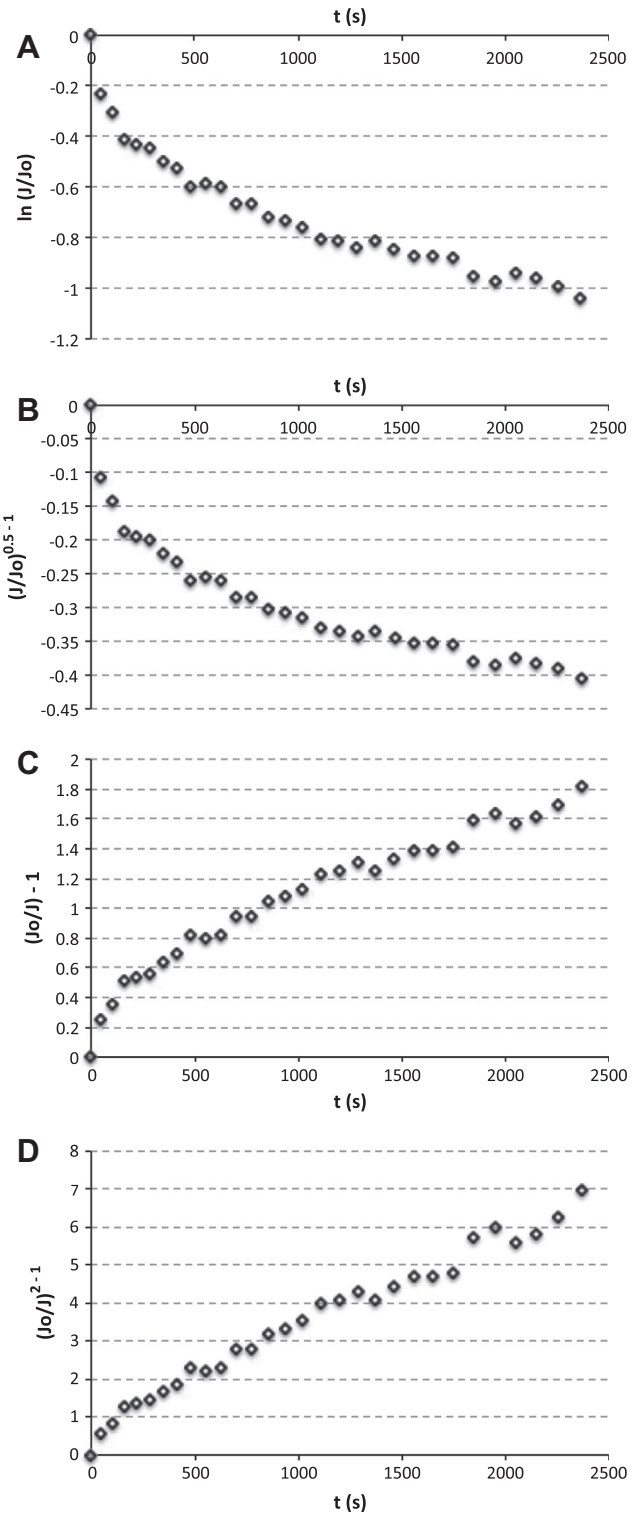



**Fig. 11.** Analysis of the BSA + SA filtration experiments from the linear expressions of the classical modelling mechanisms: (A) complete blocking; (B) standard blocking; (C) intermediate blocking; and (D) cake filtration. $R^2$ coefficients correspond to the linear regression fitting of the solid marker data points.

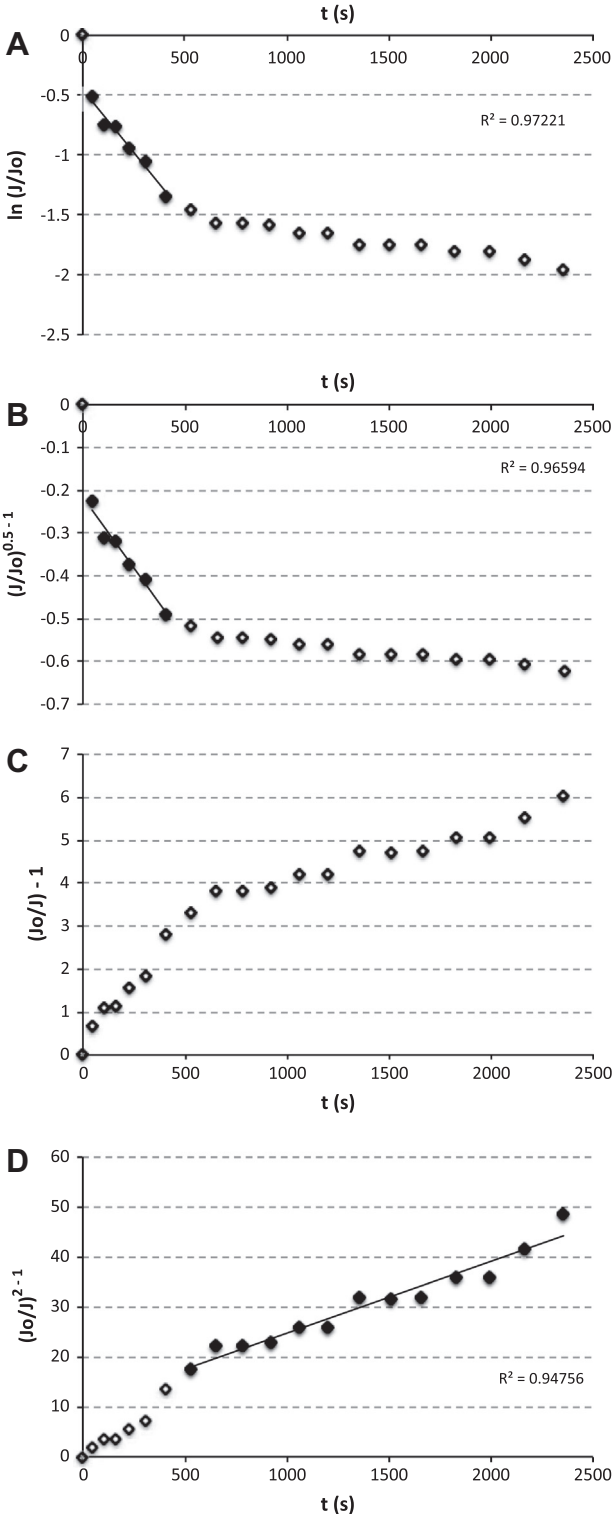



**Fig. 12.** Analysis of the BSA + HA filtration experiments from the linear expressions of the classical modelling mechanisms: (A) complete blocking; (B) standard blocking; (C) intermediate blocking; and (D) cake filtration. $R^2$ coefficients correspond to the linear regression fitting of the solid marker data points.

Author's personal copy



effect of these mixtures will determine the fouling characteristics of the solution.

Filtration experiments were conducted at concentrations of 5 ppm, 500 ppm, and 5 ppm for SA, BSA, and HA respectively, as shown in Fig. 10A1, B1 and C1. The concentration levels were chosen in order to cause low to moderate fouling within the first 250 ml filtered, and in the individual case of SA, to avoid the rapid cake formation due to the formation of the gel that was observed for a feed concentration of 10 ppm. The compounds were dissolved in ultrapure DI water and pH adjusted to 7, by addition of NaOH. Fouling layer resistance was calculated from the flux data and the clean membrane resistance. Hydraulic resistances due to fouling from each individual compound separately were compared with mixture fouling resistance and presented in Fig. 10A2, B2 and C2.

Synergism was observed during the filtration of all NOM mixtures. The flux profile observed for the BSA + SA mixture (Fig. 10A1) was very similar to that of the protein alone, and the decrease of permeate flux only slighter higher. This was in part expected, since the concentration of BSA in the mixture is 100 times that of SA, and therefore the former would be much likely to reach and adsorb on the membrane surface, relegating to a lesser degree the potential fouling effect of SA. The foulant layer resistance ($R_f$, Eq. (9)) of combined SA + BSA was compared with the sum of the individual foulant resistance of SA and BSA (Fig. 10A2). The sum of the individual resistances was somewhat less than the mixture resistance, which suggests a weak synergistic effect. This was also observed by other researchers, investigating SA–BSA fouling of polymeric membranes [27]. A comparison of the modelled flux declined by fouling mechanisms of the BSA and mixture experiments, showed that while the curves highly resemble the BSA-alone situation, a shift from the early standard blocking mechanism can be seen when SA is present. A depart from the original linear form, evidenced in Fig. 6 for BSA only experiment, can be observed in the initial stage of the filtration in Fig. 11B. This indicates that although total flux decline was not significantly changed, the presence of SA, even at low relative concentration, modified the mechanism of fouling, accelerating the particle–particle deposition phase and the onset of cake filtration.

Opposite to these findings, the filtration of a 500 ppm protein and 5 ppm HA solution was greatly affected by the presence of the minor component, as demonstrated by the flux declined curve in Fig. 10B1. After filtering 200 ml, flux decline reached almost 90%, while single foulants caused only a 50% decrease in permeability. The calculated resistance due to fouling shown in Fig. 10B2 also evidenced an important rise from the added resistances exerted by the compounds when filtrated individually. Mechanistically, the strong influence of HA in the mixture was manifested through the modelling of the flux data presented in Fig. 12. Similar to HA (Fig. 5A and B) and in contrast to BSA modelled data (Fig. 6A and B), an abrupt change of dominant fouling mechanism after 500 s, corresponding to approximately 80 ml of permeate obtained, was observed for the mixture (Fig. 12A and B). Complete blocking best represented the initial mechanism whereas, after the mentioned divide, cake formation appeared to be the prevalent one. Foulant–membrane interactions must be responsible for the changes observed, since it is at the early stages of the filtration when they are most relevant, while foulant–foulant interactions are likely to act when the membrane surface become covered. BSA negative charge density expected to be higher than HA at the working pH. Since iron oxide will also be negatively charged, electrostatic repulsion may result in relatively larger concentration of HA near the surface and in turn, favour the adsorption of the hydrophobic component. The fouling potential of the cake formed by the mixture showed significant synergy compared to separate filtrations. The HA molecules become trapped in protein polymeric structure, becoming part of the cake arrangement [19,34]. This is mainly attributable to chemical interactions between the hydrophobic parts of the macromolecules, whose polymeric carbonic chains can deform in space so as to clog the HA molecules, resulting in more compact, less permeable cake.

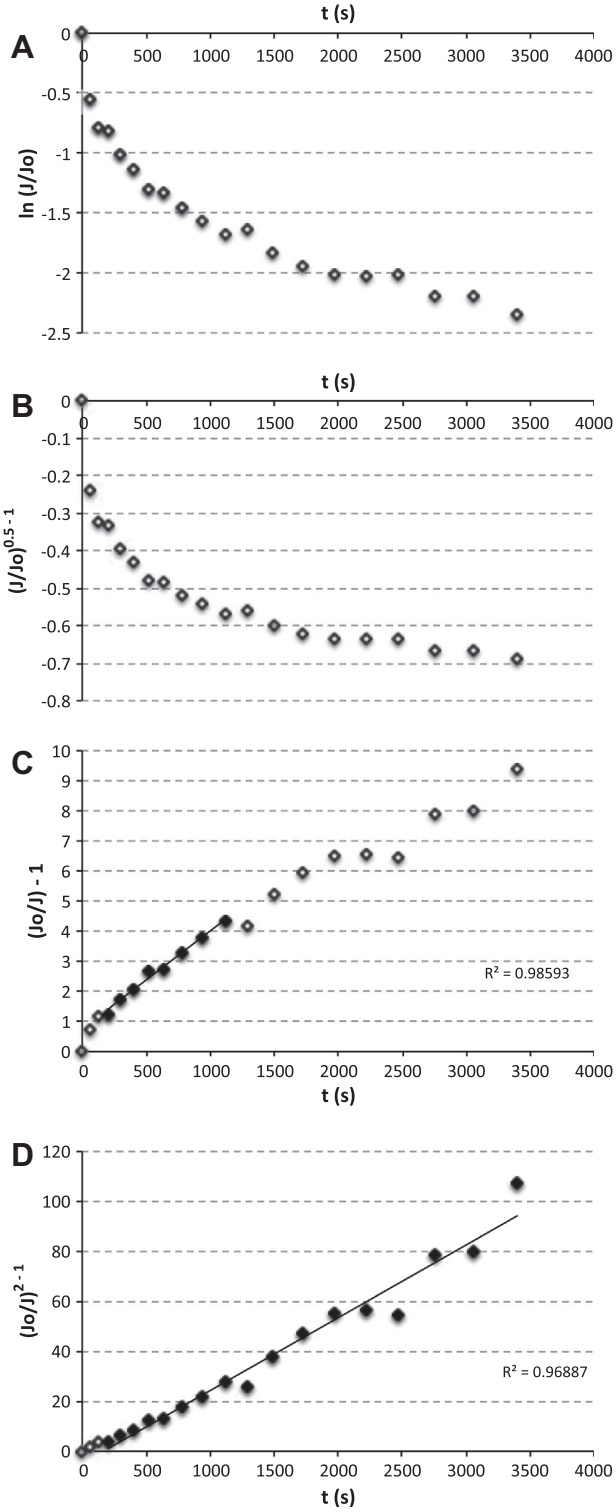



**Fig. 13.** Analysis of the HA + SA filtration experiments from the linear expressions of the classical modelling mechanisms: (A) complete blocking; (B) standard blocking; (C) intermediate blocking; and (D) cake filtration. $R^2$ coefficients correspond to the linear regression fitting of the solid marker data points.

Author's personal copy



Finally, fouling potential of a mixture of equal mass concentration of HA and SA was investigated. The observed flux reduction was also significantly higher than for the SA–BSA mixture (Fig. 10C1). Although the components at the studied concentrations in separate filtrations were the ones causing the least fouling, its combined effect was the worst of the three situations tested. The observation can be interpreted as HA being incorporated into the alginate gel layer while it was formed, developing a less porous cake. The interpretation is further supported by analysis of the fouling mechanisms involved. The linear fitting to the four classical mechanisms presented in Fig. 13, indicated a first period of intermediate layer followed rapidly by cake filtration; thus, the mixture behaves mechanistically similarly to pure alginate, with the added resistance due to entrapment of HA molecules into the otherwise porous SA gel layer. Analysis of fouling layer resistance showed an enhanced $R_f$ growth during combined fouling experiments, which implied a strong synergistic effect when SA was co-filtered with HA. (Fig. 10C2).

*4.2.3. Effect of solution pH on fouling potential*

The pH of the solution can have an influence in both structure and charge of the molecules in solution as well as the charge of the membrane surface, affecting foulant–foulant and foulant–membrane interactions.

In order to study the influence of pH in the fouling characteristics, experiments were performed at pH values of 5 and 7.5 for HA and SA, and 3, 4.7, 6, and 7.5 for BSA. Although pH 3 is not common in natural waters, it was studied for being below the isoelectric point of the protein. The foulant concentrations were 5 ppm, 500 ppm, and 5 ppm for HA, BSA, and SA respectively. The solutions were adjusted to working pH using HCl or NaOH.

The charge conditions for all foulants and membrane material is summarized in Table 1 for all conditions tested [36,10,37].

HA molecules have a number of different acidic functional groups such as carboxylic acids, and phenols. Depending on the acidity of the NOM source, HA molecules will exhibit different charge density at each pH. While phenolic groups will be predominantly non-ionized at the pHs considered in this work (below 8), carboxylic groups can be expected to be only partially ionized for pH < 6 [38]. Therefore, HA is expected to be negatively charged under the conditions tested, although an increase in surface ionized groups is anticipated for the higher pH investigated. At pH 5 there was a significant initial flux decline, followed by a steady decrease in $J/J_0$ with a slope similar to that observed at pH 7.5 (Fig. 14A). This may be due to the fact that at pH 5, the membrane surface charge is opposite to the HA net charge, and although carboxylic acids would be only partially ionized at the working pH, an electrostatic attractive force was present and increased the fouling effect by drawing the molecules to the surface. Furthermore, due to the protonation of humic acid functional group –COOH and the decrease in the net charge, an increase in hydrophobicity of the humic molecules is expected, and hence a higher tendency to adsorb on the iron oxide driven by the hydrophobic effect [39]. At pH 7.5, there was an electrostatic repulsive force between HA molecules, provided by the completely deprotonated carboxylic groups, and the membrane surface, since they both were negatively charged and, therefore, the first stage of fouling due to attractive membrane–foulant interactions was absent.

The IEP of BSA and the pzc of the membrane (Table 1) determine different pH ranges with respect to the fouling characteristics due to electrostatic protein–membrane interaction. For pHs lower than 4.7 and higher than 6.5, the membrane and BSA have both the same charge and the electrostatic repulsions will play a role. Alternatively, for pHs between 4.7 and 6.5, a situation arises when one is charged and the other has a net charge close to zero, and due to the absence of electrostatic repulsion, fouling is expected to be more pronounced. Flux profiles obtained under pHs 3 and 7.5 were similarly shaped (Fig. 14B); these conditions correspond to same net charge of membrane surface and foulant and therefore repulsion is expected. Filtrations in the absence of electrostatic

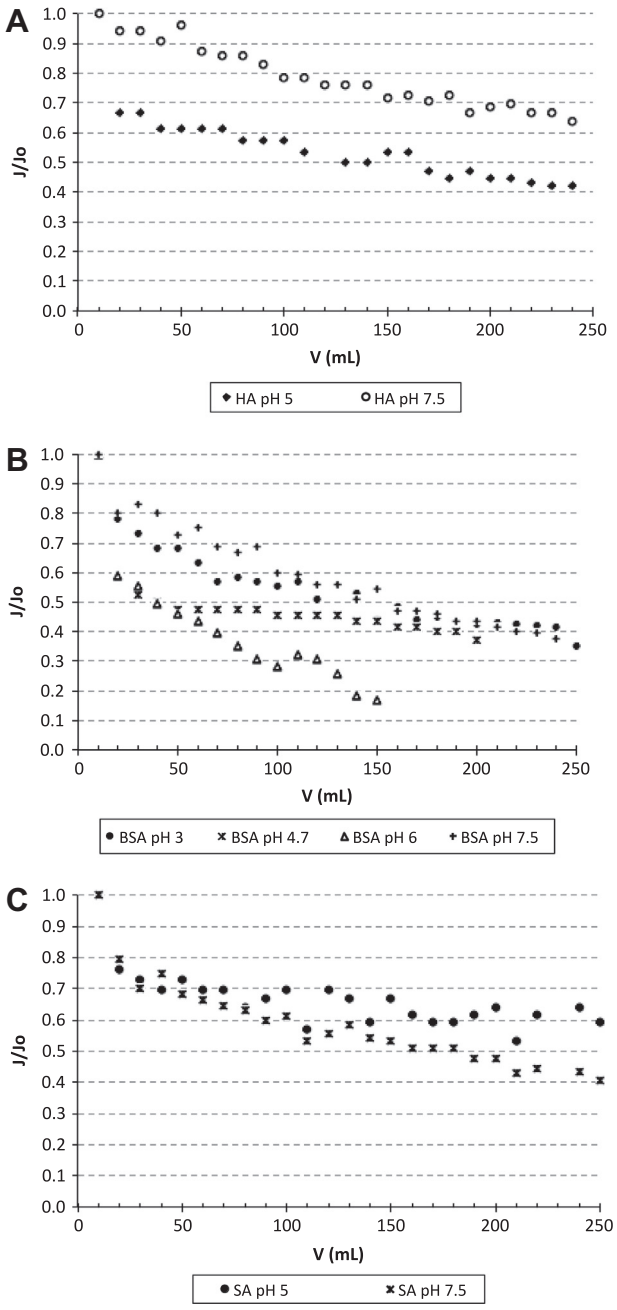



**Fig. 14.** Normalized permeability vs. pH feed solution for: (A) HA (5 ppm); (B) BSA (500 ppm); and (C) SA (5 ppm); $\Delta P = 0.5$ bar.

**Table 1**
Net charge for molecules and membrane for the conditions investigated (N/A: not applicable).

| pH | Membrane (pzc = 6.3) | HA (pK~3–4)[36] | BSA (IEP = 4.7)[10] | SA (pK~4–5)[37] |
|---|---|---|---|---|
| 3 | + | N/A | + | N/A |
| 4.7 | + | N/A | No charge | N/A |
| 5/6 | + | – | – | – |
| 7.5 | – | – | – | – |

Author's personal copy



repulsion forces also shared a similar profile for the initial part of the experiment. Interestingly, the filtration performed at the IEP of the protein did not result in a more accentuated flux reduction than the previous two cases. The worst scenario was determined to be when membrane and solute had opposite charges, and an attractive force developed. In summary, repulsion forces demonstrated to be effective in retarding the flux decay through iron oxide membranes, but could not prevent significant fouling to occur, most probably due to adsorption as suggested by the large irreversible fraction observed under similar conditions (Fig. 4). At pH 4.7, the uncharged protein produced a faster reduction of flux, indicating a rapid accumulation of foulant near or at the positively charged membrane. After this initial stage, filtration follows the same pattern than the previous cases, further substantiating the hypothesis that chemical affinity dominated over repulsion forces in BSA filtration by iron oxide membranes. Electrostatic effects usually dominate adsorption of organics on iron oxides, although hydrogen bonding is also involved [25]. Fouling was worst when solute and membrane were oppositely charged, as retention should be the highest: in fact, De la Casa et al. (2008) found absolutely no transmission of BSA through an alumina tubular membrane at pH 6 [10].

For SA experiments, in all conditions investigated (pH 5 and 7.5), the polysaccharide was negatively charged; in contrast to HA, the difference found in the SA is not significant between the two pHs examined (Fig. 14C). Fouling by SA was largely directed by intermolecular interactions, rather than membrane–foulant interactions, as evidenced by the analysis of mechanisms presented in Section 4.3, where cake filtration is predominant. The gel formation and cake porosity is not expected to suffer modifications under the pHs investigated, and therefore no differences are observed in the experimental results.

## 5. Conclusions

All organic matter substances investigated in this work resulted in significant fouling of the iron oxide ceramic membranes, and the eventual formation of a cake on the membrane surface. Differences in the initial stages of the filtration experiments were identified. This is particularly interesting, since the main objective of this work was to investigate the performance of a new membrane material.

HA caused fouling through complete blocking in the initial stages, followed by intermediate blocking, while BSA main mechanism was standard blocking. HA deposited on top of the membrane, probably partially aggregated at pH 7, while BSA strongly adsorbed inside the pores. SA rapidly formed a gel layer evidenced by cake filtration.

After hydraulic washing, about 50% of the permeability loss was regained for HA and SA fouled membranes, although very little improvement was seen for BSA. Water cleaning was not completely effective in the removal of the fouling layers. The adsorption tendency and a rough surface contributed to this effect. In fact, roughness was significantly reduced after filtration and washing experiments in comparison to the original material, as observed by AFM scans.

The affinity for BSA and its fouling inside the pores resulted in the highest portion of irreversible fouling.

Additionally, resuming water filtration caused further loss of permeability through compaction of the residual cake for HA and BSA. On the other hand, SA irreversible fouling level remained constant since the gel formed kept its porosity, regardless of the moderate pressure applied. In this sense, BSA was identified as the most detrimental compound with respect to fouling.

Flux decrease was proportional to foulant concentration in HA and BSA experiments from 1 to 10 ppm and 10 to 1000 ppm respectively. SA filtration experiments at low concentrations produced a small decrease in permeability, without dependency on actual concentration level; for higher (10 ppm) levels, a concentration was reached to form the gel layer: significant fouling was expressed.

When HA was combined with the other compounds, a strong synergistic effect was evidenced. HA dominated the mechanism and caused increased fouling in combination with a much higher concentration of BSA; when co-filtered with SA, it resulted in the worst fouling situation, due to the formation of a denser, less porous cake owing to the entrapment of the HA molecules inside the SA gel.

Changes in pH are important for metal oxide surfaces, and proved to have an influence on fouling for HA and BSA. Adsorption and electrostatic repulsion had different relative importance depending on the net charge at the working pHs; however, fouling was observed in all cases, and adsorption on the membrane surface could not be completely avoided. Due to the particular mechanism and gel formation property of SA, no dependency on filtration pH could be determined for the polysaccharide.

In summary, while iron oxides have a tendency to adsorb organic compounds, the effect was much accentuated in the case of BSA, due to the hydrophilic nature of the functional groups in the molecule and the iron oxides. Surface modifications that increase the hydrophobicity of the membrane surface may be required in order to lessen the degree of fouling in the case of feed solutions with high concentrations of polar organic compounds. Surface roughness also played a role in preventing a complete removal of the contaminants from the membrane surface during hydraulic cleaning and increasing irreversible fouling, which may lead to the need of a more frequent chemical cleaning. Therefore, an inexpensive and non-aggressive strategy for chemical cleaning of this membrane material should be developed in order to apply iron oxide ceramic membranes in water treatment systems.

## Acknowledgement

We acknowledge the financial support from the Agencia Nacional Científica y Tecnológica, PICTO-ITBA 31226-257. We are grateful to the Centro de Microscopías Avanzadas, FCEyN, Universidad de Buenos Aires and Museo Argentino de Ciencias Naturales "Bernardino Rivadavia" for the SEM and AFM images.

## Appendix A. Supplementary material

Supplementary data associated with this article can be found, in the online version, at http://dx.doi.org/10.1016/j.seppur.2013.08.016.

## References

[1] L. van Dijk, G.C.G. Roncken, Membrane bioreactors for wastewater treatment: the state of the art and new developments, Water Science and Technology 35 (1997) 35–41.
[2] F. Meng, B. Liao, S. Liang, F. Yang, H. Zhang, L. Song, Morphological visualization, componential characterization and microbiological identification of membrane fouling in membrane bioreactors (MBRs), Journal of Membrane Science 361 (2010) 1–14.
[3] A. Pollice, A. Brookes, B. Jefferson, S. Judd, Sub-critical flux fouling in membrane bioreactors—a review of recent literature, Desalination 174 (2005) 221–230.
[4] E. Aoustin, A.I. Schäfer, A.G. Fane, T.D. Waite, Ultrafiltration of natural organic matter, Separation and Purification Technology 22–23 (2001) 63–78.
[5] W. Yuan, A.L. Zydney, Humic acid fouling during microfiltration, Journal of Membrane Science 157 (1999) 1–12.

Author's personal copy



[6] J. Cho, G. Amy, J. Pellegrino, Membrane filtration of natural organic matter: comparison of flux decline, NOM rejection, and foulants during filtration with three UF membranes, Desalination 127 (2000) 283–298.
[7] A.W. Zularisam, A.F. Ismail, M.R. Salim, M. Sakinah, O. Hiroaki, Fabrication, fouling and foulant analyses of asymmetric polysulfone (PSF) ultrafiltration membrane fouled with natural organic matter (NOM) source waters, Journal of Membrane Science 299 (2007) 97–113.
[8] S.A. Mourouzidis-Mourouzis, A.J. Karabelas, Whey protein fouling of microfiltration ceramic membranes—pressure effects, Journal of Membrane Science 282 (2006) 124–132.
[9] D. Chen, M. Columbia, Enzymatic control of alginate fouling of dead-end MF and UF ceramic membranes, Journal of Membrane Science 381 (2011) 118–125.
[10] E.J. de la Casa, A. Guadix, R. Ibáñez, F. Camacho, E.M. Guadix, A combined fouling model to describe the influence of the electrostatic environment on the cross-flow microfiltration of BSA, Journal of Membrane Science 318 (2008) 247–254.
[11] P. Yao, K.-H. Choo, M.-H. Kim, A hybridized photocatalysis–microfiltration system with iron oxide-coated membranes for the removal of natural organic matter in water treatment: effects of iron oxide layers and colloids, Water Research 43 (2009) 4238–4248.
[12] S.H. Davies, M.J. Baumann, S. Byun, L.M. Corneal, V.V. Tarabara, S.J. Masten, Fabrication of catalytic ceramic membranes for water filtration, Water Science and Technology: Water Supply—WSTWS 10 (2010) 81–86.
[13] B.I. Harman, H. Koseoglu, N.O. Yigit, M. Beyhan, M. Kitis, The use of iron oxide-coated ceramic membranes in removing natural organic matter and phenol from waters, Desalination 261 (2010) 27–33.
[14] H. Park, Y. Kim, B. An, H. Choi, Characterization of natural organic matter treated by iron oxide nanoparticle incorporated ceramic membrane-ozonation process, Water Research 46 (2012) 5861–5870.
[15] V.A. Hackley, M.A. Anderson, Synthesis and characterization of unsupported ferric oxide ceramic membranes, Journal of Membrane Science 70 (1992) 41–51.
[16] H. Lee, G. Amy, J. Cho, Y. Yoon, S.-H. Moon, I.S. Kim, Cleaning strategies for flux recovery of an ultrafiltration membrane fouled by natural organic matter, Water Research 35 (2001) 3301–3308.
[17] C. Jucker, M.M. Clark, Adsorption of aquatic humic substances on hydrophobic ultrafiltration membranes, Journal of Membrane Science 97 (1994) 37–52.
[18] S. Hong, M. Elimelech, Chemical and physical aspects of natural organic matter (NOM) fouling of nanofiltration membranes, Journal of Membrane Science 132 (1997) 159–181.
[19] W.S. Ang, A. Tiraferri, K.L. Chen, M. Elimelech, Fouling and cleaning of RO membranes fouled by mixtures of organic foulants simulating wastewater effluent, Journal of Membrane Science 376 (2011) 196–206.
[20] M.a.M. Cortalezzi, J. Rose, G.F. Wells, J.-Y. Bottero, A.R. Barron, M.R. Wiesner, Ceramic membranes derived from ferroxane nanoparticles: a new route for the fabrication of iron oxide ultrafiltration membranes, Journal of Membrane Science 227 (2003) 207–217.
[21] P. Sabbatini, F. Rossi, G. Thern, A. Marajofsky, M.M.F. de Cortalezzi, Iron oxide adsorbers for arsenic removal: a low cost treatment for rural areas and mobile applications, Desalination 248 (2009) 184–192.
[22] I. Sentana, R.D.S. Puche, E. Sentana, D. Prats, Reduction of chlorination byproducts in surface water using ceramic nanofiltration membranes, Desalination 277 (2011) 147–155.
[23] L. Liu, Z. Liu, H. Bai, D.D. Sun, Concurrent filtration and solar photocatalytic disinfection/degradation using high-performance Ag/$TiO_2$ nanofiber membrane, Water Research 46 (2012) 1101–1112.
[24] U. Schwertmann, R.M. Cornell, Iron Oxides in the Laboratory: Preparation and Characterization, 2000.
[25] U. Schwertmann, R.M. Cornell, The Iron Oxides: Structure, Properties, Reactions, Occurrences and Uses, New York, 1996.
[26] K. Boussu, B. Van der Bruggen, A. Volodin, J. Snauwaert, C. Van Haesendonck, C. Vandecasteele, Roughness and hydrophobicity studies of nanofiltration membranes using different modes of AFM, Journal of Colloid and Interface Science 286 (2005) 632–638.
[27] Q. Li, Z. Xu, I. Pinnau, Fouling of reverse osmosis membranes by biopolymers in wastewater secondary effluent: role of membrane surface properties and initial permeate flux, Journal of Membrane Science 290 (2007) 173–181.
[28] V. García-Molina, S. Lyko, S. Esplugas, T. Wintgens, T. Melin, Ultrafiltration of aqueous solutions containing organic polymers, Desalination 189 (2006) 110–118.
[29] W.R. Bowen, J.I. Calvo, A. Hernández, Steps of membrane blocking in flux decline during protein microfiltration, Journal of Membrane Science 101 (1995) 153–165.
[30] C.-C. Ho, A.L. Zydney, A combined pore blockage and cake filtration model for protein fouling during microfiltration, Journal of Colloid and Interface Science 232 (2000) 389–399.
[31] M. Kawahigashi, H. Sumida, K. Yamamoto, Size and shape of soil humic acids estimated by viscosity and molecular weight, Journal of Colloid and Interface Science 284 (2005) 463–469.
[32] A. Persson, A.-S. Jönsson, G. Zacchi, Transmission of BSA during cross-flow microfiltration: influence of pH and salt concentration, Journal of Membrane Science 223 (2003) 11–21.
[33] M. Hashino, K. Hirami, T. Katagiri, N. Kubota, Y. Ohmukai, T. Ishigami, T. Maruyama, H. Matsuyama, Effects of three natural organic matter types on cellulose acetate butyrate microfiltration membrane fouling, Journal of Membrane Science 379 (2011) 233–238.
[34] D. Jermann, W. Pronk, S. Meylan, M. Boller, Interplay of different NOM fouling mechanisms during ultrafiltration for drinking water production, Water Research 41 (2007) 1713–1722.
[35] N. Lee, G. Amy, J.-P. Croué, H. Buisson, Morphological analyses of natural organic matter NOM) fouling of low-pressure membranes (MF/UF), Journal of Membrane Science 261 (2005) 7–16.
[36] G.R. Aiken, M.D. Mcknight, R.L. Wershaw, P. Mc Carthy, Humic substances in soil, Sediment and Water – Geochemistry Isolation and Characterization, New York, 1985.
[37] F.A. Simsek-Ege, G.M. Bond, J. Stringer, Polyelectrolyte complex formation between alginate and chitosan as a function of pH, Journal of Applied Polymer Science 88 (2003) 346–351.
[38] M.R. Collins, G.L. Amy, C. Steelink, Molecular weight distribution, carboxylic acidity, and humic substances content of aquatic organic matter: implications for removal during water treatment, Environmental Science and Technology 20 (1986) 1028–1032.
[39] W. Stumm, L. Sigg, B. Sulzberger, Chemistry of the Solid-Water Interface: Processes at the Mineral-Water and Particle–Water Interface in Natural Systems, Wiley, 1992.